MOVPE growth of GaP/GaPN core-shell nanowires: N incorporation, morphology and crystal structure

Matthias Steidl[1*], Klaus Schwarzburg[2], Beatriz Galiana[3], Thomas Kups[4], Oliver Supplie[1], Peter Kleinschmidt[1], Gerhard Lilienkamp[5], T. Hannappel[1*]

[1]Department of Photovoltaics, Institute of Physics and Institute of Micro- and Nanotechnologies, Technische Universität Ilmenau, 98693 Ilmenau, Germany
[2]Department Nanoscale Structures and Microscopic Analysis, Helmholtz Zentrum Berlin, 14109 Berlin, Germany
[3]Physics Department, Universidad Carlos III de Madrid (UC3M), 28911, Madrid, Spain
[4]Department of Materials for Electronics, Institute of Materials Science and Engineering, Technische Universität Ilmenau, 98693 Ilmenau, Germany
[5]Institute of Energy Research and Physical Technologies, Technische Universität Clausthal, 38678 Clausthal, Germany

*E-mail: matthias.steidl@tu-ilmenau.de, thomas.hannappel@tu-ilmenau.de

Received xxxxxx
Accepted for publication xxxxxx
Published xxxxxx

Abstract

Dilute nitride III-V nanowires (NWs) possess great potential as building blocks in future optoelectronical and electrochemical devices. Here, we provide evidence for the growth of GaP/GaPN core-shell NWs via metalorganic vapor phase epitaxy (MOVPE), both on GaP(111)B and on GaP/Si(111) hetero-substrates. The NW morphology meets the common needs for use in applications, i. e. they are straight and vertically oriented to the substrate as well as homogeneous in length. Moreover, no parasitical island growth is observed. Nitrogen was found to be incorporated on group V sites as determined from transmission electron microscopy (TEM) and Raman spectroscopy. Together with the incorporation of N, the NWs exhibit strong photoluminescence in the visible range, which we attribute to radiative recombination at N-related deep states. Independently of the N incorporation, a peculiar facet formation was found, with {110} facets at the top and {112} at the bottom of the NWs. TEM reveals that this phenomenon is related to different stacking fault densities within the zinc blende structure, which lead to different effective surface energies for the bottom and the top of the NWs.

Keywords: III-V on silicon, nanowires, dilute nitride, MOVPE, facet formation, optical spectroscopy

1. Introduction

III-V nanowires (NWs) are considered to be very promising as device components, not only for the new generation of optoelectronic devices such as solar cells [1,2], LEDs [3], lasers [4,5], or photodetectors [6,7], but also for chemical sensors [8] and photoelectrochemical cells [9,10]. Their one dimensional geometry gives rise to several benefits: The small footprint, for instance, allows for efficient strain relaxation [11] and, in turn, significantly mismatched heterostructures with high crystal quality. Their high aspect ratio enables efficient light absorption [12] and emission [13] while (lateral) charge transfer distances are short. Furthermore, the high surface-to-volume ratio is beneficial for surface reactive devices.

The incorporation of small fractions of nitrogen into III-V semiconductors enables further tailoring of the NW material properties via band structure and lattice engineering [14]. Diluted N incorporation into GaP, for example, strongly affects the magnitude and nature of the bandgap [15,16]. Furthermore, alloying with N improves the chemical stability of GaAs, GaP and GaInP against photocorrosion in aqueous solutions [17,18], which is particularly attractive for solar water splitting.

Pioneering work on dilute nitride NW growth was performed by Seo et al. in 2003 utilizing NH_3 to dope GaP-NWs with N during the growth on alumina substrates via

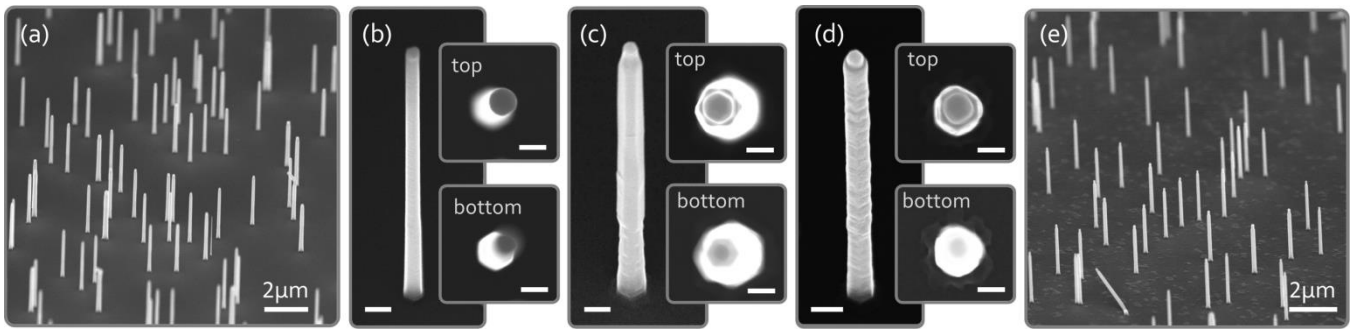

Fig. 1: (a) GaP/GaPN core-shell NWs on GaP(111)B. (b) GaP NW without shell, (c) GaP NW with GaPN-shell grown with a UDMH:TBP ratio of 2, and (d) with a UDMH:TBP ratio of 4; the respective insets show top views focused on the top or the bottom to visualize the different side facets. Images (b,c,d) have the same orientation. (e) GaP/GaPN core-shell NWs on GaP/Si(111) prepared according to Ref. [25]. Images (a) and (e) are recorded under 45° tilt, and images (b), (c) and (d) under 30° tilt. Scale bars in (b-d) are 200 nm for the tilted views and 100 nm for the top views.

sublimation and recondensation of GaP powder [19]. They observed a strong increase in photoluminescence (PL) intensity compared to undoped GaP NWs. However, high growth temperatures of 950 °C were used and there was no epitaxial relation to the growth substrate. Subsequent research focused on molecular beam epitaxy (MBE) of GaPN and GaAsN NW structures, which were found to exhibit advances over comparable planar structures: Reduction of detrimental surface recombination processes by incorporation of N into GaAs [20]; increased light harvesting in GaP(N) via energy up conversion caused by two-step two photon absorption processes [21]; emission of light, linearly polarized perpendicular to the wire axis due to the presence of N and planar defects [22,23]. In comparison to MBE, growth by metal organic vapor-phase epitaxy (MOVPE) would be beneficial with regard to cost and scalability at industrially relevant level. So far, the only attempts reported in the literature to grow dilute nitride NW structures via MOVPE have failed [24].

In this work, we establish the growth of dilute nitride NW structures via MOVPE: GaP/GaPN core-shell NWs are grown on both GaP(111)B and GaP/Si(111) hetero-substrates [25,26]. We present complementary approaches to quantify the N content in single NWs which are based on Raman spectroscopy and transmission electron microscopy (TEM). The impact of N incorporation on morphology, crystal structure, vibrational and optical properties of the NWs are studied by scanning electron microscopy (SEM), TEM, µ-Raman and µ-PL spectroscopy, respectively.

2. Experimental

The NW structures were grown in a horizontal MOVPE reactor (Aixtron AIX 200) utilizing H_2 as carrier gas and trimethylgallium (TMGa), tertiarybutylphosphine (TBP), and unsymmetrical dimethylhydrazine (UDMH) as precursors for Ga, P, and N, respectively. Prior to NW growth, the substrates were cleaned in acetone and isopropyl alcohol, and Au particles of 100 nm in diameter were deposited on them from colloidal solution. To desorb the surface oxide and to form eutectic Au-Ga droplets, the samples were loaded into the reactor and annealed for at least 5 minutes at 550 °C or 600 °C under flow of TBP. Then, GaP NW cores were grown via the Au-mediated vapor-liquid-solid (VLS) mechanism at 500 °C for 10 minutes with a molar fraction of $\chi_{TMGa} = 6.16 \times 10^{-5}$ and a TBP/TMGa ratio of 10. Growth of GaP(N) shells was carried out for 3 minutes at 625°C with equal TMGa and TBP flows, but supplying UDMH with UDMH:TBP ratios ranging from 0 to 4. For some samples an additional GaP-shell was grown for 1 minute. The GaP/Si(111) hetero-substrate was prepared according to ref. [25] with a nucleation temperature of 420°C leading to a twin ratio below 8%. All temperatures mentioned are measured by a thermocouple within the graphite suszeptor.

All samples were characterized by means of high resolution scanning electron microscopy (SEM, Hitachi S 4800-II). Transmission electron microscopy was applied to investigate the crystal structure of selected GaP/GaPN/GaP core-multishell NWs. It was performed on a FEI 200 kV scanning/transmission electron microscope (S/TEM). Lamellas of the samples were prepared by means of a focused ion beam (FIB). For the µ-Raman and -PL characterization, NW samples were (mechanically) dry-transferred on Si or quartz glass substrates. A green 532 nm laser with 400 µW was used as the excitation source and focused with a 50x objective. The signal was analyzed with a 550 mm focal length spectrometer using a 1200 l/mm grating and a cooled Si CCD detector.

3. Results and discussion

3.1 Morphology and structure analysis

Fig. 1 shows representative SEM scans of differently prepared NW structures. Panel (a) and (e) present GaP/GaPN core-shell NWs grown on GaP(111)B and GaP/Si(111) hetero-substrates, respectively. In both cases, almost all NWs are straight and vertically oriented to the substrate surface,

i.e. pointing in the [111]B direction; besides, no parasitic islands or comparable structures are observed, which are prevalent for self-catalyzed MBE-growth of NWs [27,28]. This likely is a consequence of the lower growth temperature and the presumably higher diffusion lengths during MOVPE growth. This observation is true over the entire sample surface and an important prerequisite for potential application in devices. Furthermore, the NWs have a narrow length (3.48±0.07 µm) and thickness distribution (208±11 nm at the top), which do not correlate with each other. Diagonal NWs, such as the one indicated by an arrow in panel (e), are only observed for the GaP/Si substrates and are caused by rotational twins within the heteroepitaxial GaP-layer [26]. Note that the rather low NW density can easily be increased by depositing more gold particles or by the use of evaporated Au-layers (1-2 nm thickness) instead.

Fig. 1 (b) shows a representative single VLS-grown GaP NW without shell overgrowth. At the bottom it exhibits a hexagonal cross section with {112} facets, where the distance between opposite facets is ~140 nm. At the top, in contrast, the cross section is almost circular with a diameter of about 100 nm, i.e. the NW is slightly tapered. After 3 minutes growth of a GaPN shell with an intermediate UDMH:TBP ratio of 2 (Fig. 1 (c)) the diameter increases to around 210 nm at the top and around 260 nm at the bottom. Hence, the shell thickness measures about 50 nm. The ~250 nm long tapered neck directly below the Au particle shows that VLS growth was not entirely suppressed during shell growth.

An interesting phenomenon is the unusual shape of the side facets extending along the NW after shell growth, which is observed both for pure GaP shells and GaPN shells grown with intermediate UDMH:TBP ratios (ranging from 0 to 3). Here, the upper part of the NW exhibits smooth, well-pronounced {110}-facets, while the bottom part preferentially forms {112} facets with a comparably rough surface. For UDMH:TBP = 4, these rough {112} facets extend over the entire NW (Fig. 1(d)). In order to confirm this assignment and to exclude a hypothetical rotation of the lattice by 30°, TEM on cross sections of the upper and the lower part was carried out. The investigated NW was grown with UDMH:TBP = 2 and possesses an outer GaP-shell, which does not alter the facet formation as it can be seen in Fig. 2(a). Since the FFTs of HRTEM scans of the upper (d') and the lower part (d'') exhibit spots at equal positions, it is evident that the upper and the lower part possess the same lattice orientation, in agreement with the facet assignment. Additionally, overview scans reveal that the upper part indeed consists only of {110} facets, whereas the lower part exhibits both wide {112} facets and narrow {110} facets.

In order to understand this peculiar facet formation, axial cross sections (i. e. along the NW length axis) of the same NW type were investigated by TEM along the [1-10] zone axis. Fig. 3(a) shows an overview darkfield image of the entire NW where an {022} reflex is imaged. Accordingly, bright contrast corresponds to zinc blende (ZB) with a certain orientation. Significant differences in the contrast at the upper (yellow) and the lower (green) part can be seen (despite long range bending of the lamella). While the upper part (Fig. 3(b)) exhibits a streaky contrast, it is speckled for the lower part (Fig. 3(c)). This strongly indicates structural differences, which become evident by HRTEM at the respective positions. HRTEM across the upper part (e.g. Fig. 3(d) and (e)) and corresponding Fast Fourier Transform (FFT) images reveal that the NW exhibits pure ZB structure with some stacking faults (SFs) in this region.

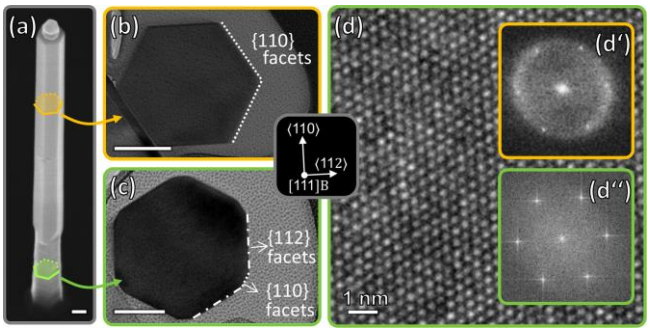

Fig. 2: Electron microscopy of GaP/GaPN/GaP core-multishell NWs, where the inner GaPN-shell measures roughly 50 nm and the outer GaP-shell about 15 nm. The UDMH:TBP ratio was 2. (a) SEM image with 30° tilt. TEM of cross sections from the upper (b) and the lower (c) NW part exhibiting different side facets. (d) HRTEM of the GaPN-shell at the lower NW part together with its corresponding Fast Fourier Transforms (FFTs) in (d''). (d') shows the FFT of an HRTEM image of a (slightly misaligned) cross section at the upper part. The scale bars in (a-c) are 100 nm.

In contrast to the upper NW part, the lower part exhibits the ZB structure with a much higher stacking fault density (Fig. 3(e)). As the different facet formation is in perfect accordance with the different SF densities, it can be concluded that the preferred facet type depends on the SF density. In addition, the facet formation does not depend on the growth time or thickness of the shell (not shown here) and, hence, appears not to be kinetically but energetically driven. It is well known that at higher temperature (above 600 °C) for ZB NWs the preferred facet type is {110} [29,30], which is a result of the higher specific surface energy of the {112} facets compared to the {110} facets [31,32]. From VLS-grown NWs, it is known that their {112} facets tend to undergo microfaceting. The {112} typically comprises {111}, {100} and {113} facets [30]. Among these, {111} facets have the lowest surface energy [31], but for geometrical reasons {100} and {113} facets are coexistent [30]. This necessity is absent, when SFs are introduced and (low energy) {111} facets alone can reproduce a {112} facet [33,34]. In analogy we argue for shell growth that microfaceted {112} surfaces can be

energetically favorable over {110} facets, if sufficient SFs are present to allow for {111} facets only: To account for the 19° inclination of the {111} facets with respect to the {112} facets a correction factor of $\cos^{-1}$ (19°) is used, yielding an

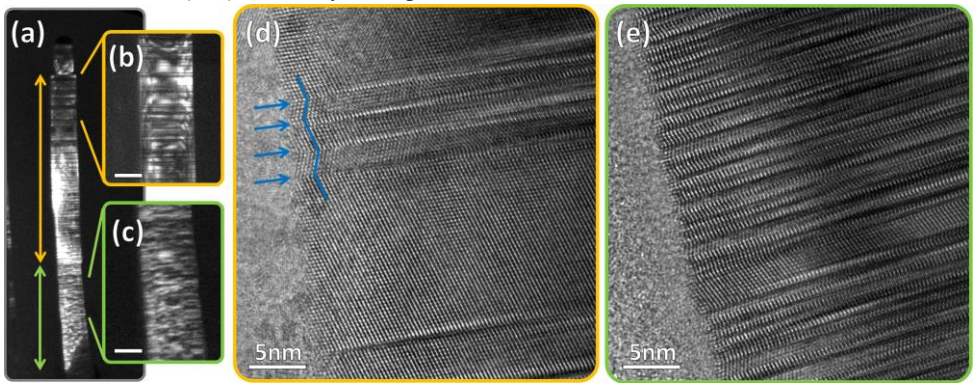

Fig. 3: TEM investigation of the length section of a GaP/GaPN/GaP core-multishell NW along the [1-10] zone axis (the NW is comparable to the ones in Fig. 2). (a) Overview darkfield image of the 220-reflex. The insets show close-ups within the upper (c) and the bottom part close to the substrate (d). HRTEM images reveal the ZB structure with moderate stacking fault (SF) density in the upper part (d) and high SF density at the bottom (e). Some of the SFs are indicated with blue arrows. The scale bars in (b) and (c) are 100 nm.

effective surface energy of $\gamma_{112,\mu\text{-faceted}} = \gamma_{111,\text{eff}} = \cos^{-1}$ (19°) × 1.69 Jm^{-2}=1.79 Jm^{-2} for GaP [31]. This value is considerably lower than for {110} facets (2.06 Jm^{-2} [31]) and hence microfaceted {112} facets are preferred, if the SF density is high enough. Note that a {111} microfaceting of the {112} facet can indeed be partly observed in our TEM data (cf. Fig 3(e))). The different SF densities, in turn, are likely a result of different supersaturations during the different stages of VLS-growth [35,36] – which will be determined also by different effective V/III ratios due to limited diffusion lengths of the growth species.

In the following, FFTs from HRTEM images are analyzed and used to estimate the N content within the GaPN shell. FFTs from HRTEM images within the shell close to the edge (cf. Fig. 4(b)) show that this region comprises both GaP and GaPN, which meets expectations based on the NW geometry (cf. Fig 4(a)).

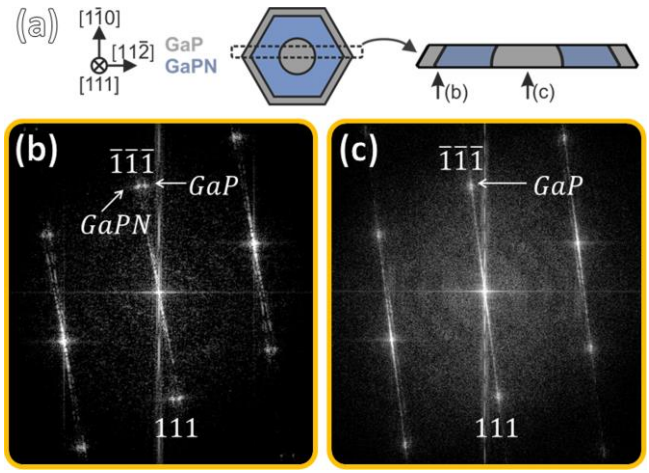

Fig. 4: (a) Sketch of the TEM lamella structure in the upper part. FFTs of HRTEM image close to the edge (b) and within the center (c). The overlap of GaP and GaPN close to the edge (b) allows for an estimation of the N content within the $GaPN_x$ shell applying Vegard's law. On average this yields x = 4.3% for the used UDMH:TBP ratio of 2.

The GaP and GaPN spots can be correctly assigned, as the {-1-1-1}/{111} spot pairs differ both in distance and orientation. The rotation angle of around 3.4° is likely a result of strain accommodation during lamella preparation due to the lattice mismatch between GaP and GaPN. When imaging the core, the GaPN related spots are absent as is expected from a TEM-lamella cut out of the NW center. Since the differences in spot distance of GaP and GaPN are significant, the N fraction within the $GaP_{1-x}N_x$ shell can be estimated applying Vegard's law. In order to reduce the variation of data, each {-1-1-1}/{111} spot pair is measured at least 3 times. Several positions on the left and on the right hand side of the NW were characterized, yielding N fractions x ranging from (2.5±0.84)% to (5.7±1.5)% with an uncertainty given by the standard error. On average, the shell contains 4.3% with a standard deviation of 1.6%. Since the GaPN might not be completely relaxed, this value indeed represents a lower limit for the N fraction. We also performed nano Auger electron spectroscopy (AES) measurements. Initial analysis of the AES data suggests an enrichment of N on the NW surface, though a thorough AES profiling of the N distribution via radial sputtering needs specific dedication in future measurements.

3.2 Vibrational and optical properties

For planar $GaP_{0.98}N_{0.02}$ layers grown lattice-matched on Si(001), it was recently found that optical transitions below the E_0 critical point energy of GaP exhibit a relatively low probability [37]. The observed redshift of the absorption edge compared to GaP was explained by quasi-localization of nitrogen-induced electronic states, which exhibit a strong phonon-photon coupling. Here, we will first discuss the

vibrational properties by resonant Raman spectroscopy carried out on individual NWs in the back scattering geometry, and employ it as a complementary technique to quantify the N content. Afterwards, we discuss the PL of the NWs.

Fig. 5 compares µ-Raman spectra of GaP/GaPN/GaP and GaP/GaP/GaP core-shell NWs with equal geometry and growth procedure (except application of UDMH), which were dry-transferred on a glass substrate. Note that these NWs correspond to the ones investigated by TEM (Fig. 2 – 4).The spectra are very similar to those of MBE-grown GaPN NWs [38]. Both spectra in Fig. 5 contain the transverse (TO) and longitudinal (LO) optical phonon modes due to the zone-center optical phonons in zinc blende GaP [39,40]. In addition, the spectrum of the GaP/GaPN core-shell wire exhibits two distinct peaks, one at 498 cm^{-1}, labeled as NLVM, and a second one at 387 cm^{-1}, referred to as LO_X.

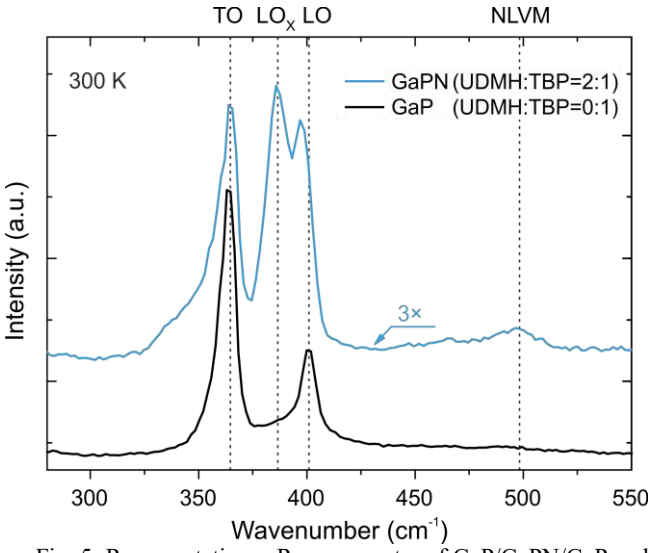

Fig. 5: Representative µ-Raman spectra of GaP/GaPN/GaP and GaP/GaP/GaP core-multishell NWs. The NWs were dry-transferred on quartz glass and measured at RT with excitation of 400 µW at 532 nm. The UDMH:TBP ratio for GaPN was set to 2.

The mode at 498 cm^{-1} originates from local vibrational modes (LVM) directly related to Ga-N bonds and therefore proves substitutional incorporation of N [39–41]. The LO_X mode is another signature of the incorporation of N; its occurrence is commonly explained by a break of the translational symmetry [40,42,43], which in our case will be caused by insertion of N into the GaP matrix. This causes relaxation of the momentum conservation rules and thereby allows zone-boundary longitudinal optical phonon scattering due to phonons at or near the X point [39,42].

Furthermore, the incorporation of N into the shell causes a shift of the LO mode from 401 cm^{-1} to 398 cm^{-1}. This frequency shift most likely originates from strain caused by different lattice constants between the GaP core and the GaPN shell [40]. The shoulder near the TO mode at around 340 cm^{-1} has only rarely been explained in the literature. Christian et al. [43] associate this mode with disorder-activated scattering (similarly to the LO_x mode), as this feature occurs both in GaPN and GaPBi with similar positions and polarization dependence.

For UDMH:TBP ratios between 0.5 and 3, Raman spectra (not shown here) exhibit the very same features, whereby the N-related characteristics, in particular the LO_X mode, get more pronounced with increasing UDMH ratio. At a UDMH:TBP ratio of 4, all N-related features get less pronounced indicating structural disorder. The LO_X phonon can be clearly observed as a fingerprint of N incorporation. However, without detailed modeling, it does not allow for a precise quantification.

In contrast, the intensity of light scattered at a specific LVM scales linearly with the concentration of impurities [44]. Hence, it is possible to quantify defect or impurity concentrations with an independent calibration. For this purpose, we measured a $GaP_{1-x}N_x$-layer as reference with a known N-content of x = 2.1% (measured via XRD) under the same conditions (not shown here) [37]. To account for the difference in the probed volume, the intensity of the NLVM is normalized to the LO mode, both for the reference and the NW sample: Fitting the spectra with Voigt functions of equal shape yields $NLVM_{Ref}/LO$ = 0.44 for the reference and $NLVM_{NW}/LO$ = 0.52 for the (entire) NW grown with UDMH:TBP = 2 for the GaPN shell (cf. Fig 5). From the linear relationship between NLVM/LO and x follows a nitrogen concentration within the entire NW of x_{NW} = 2.5%. As the GaPN-shell measures only around 55% of the NW-volume, the N-content within the GaPN-shell is $x_{GaPN\text{-}shell}$ = (4.5±1.3)%. The error is estimated from the curve fitting and deviations in the NW geometry. Note that for this estimation a homogeneous excitation of the NW volume is assumed. Indeed, absorption of the shell (estimated to be 10% for the 50 nm thick GaPN-shell), photonic modes of the NW and the coupling of the NW with the Si substrate will lead to a modified scattering amplitude. The analysis of these factors was beyond the scope of this work.

Fig. 6 juxtaposes PL spectra of individual NWs transferred to Si substrates. The investigated NWs differ in UDMH:TBP ratios during shell growth, ranging from 0 (i.e. pure GaP) to 4. The shown spectra are carefully chosen to be as representative as possible. Nevertheless, some moderate deviations were observed concerning the signal amplitude, but not the qualitative line shape. A first important observation is that the GaP/GaPN core-shell NWs up to a UDMH:TBP ratio of 3 show relatively strong PL below the bandgap of GaP at room temperature, which indicates an efficient radiative recombination. The PL intensity significantly increases with N-incorporation, reaching a maximum for UDMH:TBP ratios between 2 and 3, which

corresponds to an increase of more than two orders of magnitude compared to pure GaP. Further increase of the UMDH ratio to 4, however, quenches the PL completely, similar to the LO_X phonon observed by Raman spectroscopy. We attribute the quenched PL for UDMH:TBP = 4 to structural defects such as interstitial N atoms, vacancies and anti-sites, which are more likely to form with higher N concentration [45] and which are known to act as non-radiative recombination centers in dilute nitrides [46–48].

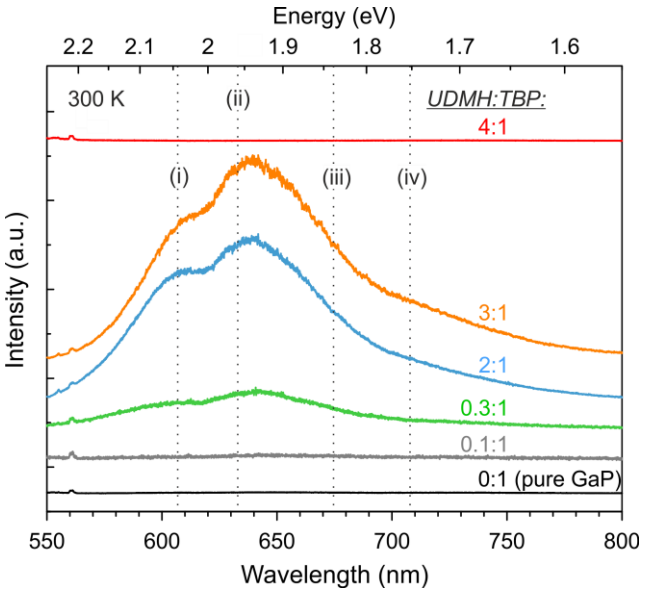

Fig. 6: Representative µ-PL spectra of GaP/GaP(N) core-shell NWs with different UDMH:TBP ratios for the shell. The NWs were dry-transferred on Si and measured at RT with excitation of 400 µW at 532 nm. For better visibility the spectra are plotted with a vertical offset. The dotted lines indicate energy positions of various N-related cluster states (taken from [52]): GaN_4 cluster (i) and 110-oriented N chains with 3 (ii), 4 (iii), and 5 (iv) nitrogen atoms.

For all samples with noticeable PL, the maximum is located at around 640 nm. Another distinctive feature is the shoulder close to 610 nm, whose relative intensity varies from NW to NW, even for NWs of the very same sample and for different positions along the same NW. Its energetic positon is also independent of the NW length so that it cannot be explained by interference effects.

Surprisingly, we observe no spectral shifts when changing the UDMH:TBP ratio. In contrast, studies on planar GaPN report on a red-shift of the maximum with increasing N incorporation [49–51], which is explained by radiative recombination of excitons trapped at various N-related localized states and an increasing N cluster size with increasing N concentration [51–56]. Band-to-band recombination, on the other hand, can be predominantly non-radiative [50,54].

The PL data in Fig. 5, thus, suggest radiative recombination stemming from specific N-related deep states — which do not change in their nature (cluster size) but increase their density with increasing UDMH:TBP ratio — in conjunction with non-radiative band-to-band recombination. The feature close to 610 nm agrees very well with Ga-centered clusters which are located up to 214 meV below the CBM [52]. In accordance, Jussila et al. as well as Peternai et al. also identify discrete spectral components at ~605 nm, which they attribute to N-clusters [45,52,57]. The position of the broad maximum at ~640 nm agrees approximately with (110)-oriented nitrogen triplets. The small discrepancy might be caused by strain induced by the GaP core, which is supported by the fact that the maximum shifts to higher wavelengths (650 nm) in case of an outer GaP shell.

4. Conclusion

We have demonstrated the growth of GaP/GaPN core-shell nanowires (NWs) via metal organic vapor-phase epitaxy. Almost all NWs have grown straight and vertically to the substrate surface and – in contrast to self-catalyzed molecular beam epitaxy – without growth of parasitic structures, both on GaP(111)B and GaP/Si(111) hetero-substrates. The NWs exhibit ZB structure and an untypical side facet formation: while the upper NW part is terminated with {110} facets (prevalent for shell growth), {112} facets prevail at the bottom of the NWs. TEM analysis revealed that this formation is directly related to the stacking fault density, which is moderate in the upper part and high in the bottom. Moreover, HRTEM and Raman spectroscopy show that N is incorporated on group V positions and can exceed composition values of several percent (2.5 – 5%). The NWs show strong photoluminescence in the visible range at room temperature, which is related to an efficient radiative combination at N-related deep states. For device fabrication, future work needs to address further process optimization with regard to defect reduction. We suggest the VS mode as a general way to achieve MOVPE growth of dilute nitride NWs and similar material systems.

Acknowledgements

This work was supported by the Deutsche Forschungs-gemeinschaft (DFG, proj. no. HA 3096/4-2 & DA 396/6-2). We thank D. Roßberg and D. Flock for preparation of the TEM lamellae via FIB, as well as A. Müller for technical support of the MOVPE system and W. Dziony for AES measurements. We appreciate fruitful discussions with A. Paszuk and A. Nägelein.

References

[1] Wallentin J, Anttu N, Asoli D, Huffman M, Aberg I, Magnusson M H, Siefer G, Fuss-Kailuweit P, Dimroth F, Witzigmann B, Xu H Q, Samuelson L, Deppert K and

Borgström M T 2013 InP Nanowire Array Solar Cells Achieving 13.8% Efficiency by Exceeding the Ray Optics Limit. *Science* **339** 1057

[2] Aberg I, Vescovi G, Asoli D, Naseem U, Gilboy J P, Sundvall C, Dahlgren A, Svensson K E, Anttu N, Bjork M T and Samuelson L 2016 A GaAs nanowire array solar cell with 15.3% efficiency at 1 sun *IEEE J. Photovoltaics* **6** 185–90

[3] Minot E D, Kelkensberg F, Van Kouwen M, Van Dam J A, Kouwenhoven L P, Zwiller V, Borgström M T, Wunnicke O, Verheijen M A and Bakkers E P A M 2007 Single quantum dot nanowire LEDs *Nano Lett.* **7** 367–71

[4] Duan X, Huang Y, Agarwal R and Lieber C M 2003 Single-nanowire electrically driven lasers *Nature* **421** 241–5

[5] Li K H, Liu X, Wang Q, Zhao S and Mi Z 2015 Ultralow-threshold electrically injected AlGaN nanowire ultraviolet lasers on Si operating at low temperature *Nat. Nanotechnol.* **10** 140–4

[6] Wang J, Gudiksen M S, Duan X, Cui Y and Lieber C M 2001 Highly Polarized Photoluminescence and Photodetection from Single Indium Phosphide Nanowires *Science (80-.).* **293** 1455–7

[7] Soci C, Zhang A, Bao X-Y, Kim H, Lo Y and Wang D 2010 Nanowire Photodetectors *J. Nanosci. Nanotechnol.* **10** 1430–49

[8] Offermans P, Crego-Calama M and Brongersma S H 2010 Gas detection with vertical InAs nanowire arrays *Nano Lett.* **10** 2412–5

[9] Sun J, Liu C and Yang P 2011 Surfactant-free, large-scale, solution-liquid-solid growth of gallium phosphide nanowires and their use for visible-light-driven hydrogen production from water reduction *J. Am. Chem. Soc.* **133** 19306–9

[10] Standing A, Assali S, Gao L, Verheijen M a., van Dam D, Cui Y, Notten P H L, Haverkort J E M and Bakkers E P a. M 2015 Efficient water reduction with gallium phosphide nanowires *Nat. Commun.* **6** 7824

[11] Glas F 2015 Strain in Nanowires and Nanowire Heterostructures *Semiconductor Nanowires I: Growth and Theory (Semiconductors and Semimetals, Volume 93)* ed A Fontcuberta i Morral, S A Dayeh and C Jagadish (Waltham, San Diego, Oxford, London: Elsevier Inc.) pp 79–123

[12] Cao L, Fan P, Vasudev A P, White J S, Yu Z, Cai W, Schuller J A, Fan S and Brongersma M L 2010 Semiconductor nanowire optical antenna solar absorbers *Nano Lett.* **10** 439–45

[13] Grzela G, Paniagua-Domínguez R, Barten T, Fontana Y, Sánchez-Gil J A and Gómez Rivas J 2012 Nanowire Antenna Emission *Nano Lett.* **12** 5481–6

[14] Ayşe E 2008 *Dilute III-V Nitride Semiconductor and Material Systems* ed E Ayşe (Berlin Heidelberg New York: Springer-Verlag)

[15] Shan W, Walukiewicz W, Yu K M, Wu J, Ager J W, Haller E E, Xin H P and Tu C W 2000 Nature of the fundamental band gap in GaNxP1-x alloys *Appl. Phys. Lett.* **76** 3251–3

[16] Buyanova I A, Pozina G, Bergman J P, Chen W M, Xin H P and Tu C W 2002 Time-resolved studies of photoluminescence in GaNxP1−x alloys: Evidence for indirect-direct band gap crossover *Appl. Phys. Lett.* **81** 52–4

[17] Deutsch T G, Koval C A and Turner J A 2006 III-V nitride epilayers for photoelectrochemical water splitting: GaPN and GaAsPN *J. Phys. Chem. B* **110** 25297–307

[18] Deutsch T G, Head J L and Turner J A 2008 Photoelectrochemical Characterization and Durability Analysis of GaInPN Epilayers *J. Electrochem. Soc.* **155** B903

[19] Seo H W, Bae S Y, Park J, Kang M and Kim S 2003 Nitrogen-doped gallium phosphide nanowires *Chem. Phys. Lett.* **378** 420–4

[20] Chen S L, Chen W M, Ishikawa F and Buyanova I A 2015 Suppression of non-radiative surface recombination by N incorporation in GaAs/GaNAs core/shell nanowires. *Sci. Rep.* **5** 11653

[21] Dobrovolsky A, Sukrittanon S, Kuang Y, Tu C W, Chen W M and Buyanova I A 2014 Energy Upconversion in GaP/GaNP Core/Shell Nanowires for Enhanced Near-Infrared Light Harvesting *Small* **10** 4403–8

[22] Filippov S, Sukrittanon S, Kuang Y, Tu C, Persson P O Å, Chen W M and Buyanova I A 2014 Origin of strong photoluminescence polarization in GaNP nanowires *Nano Lett.* **14** 5264–9

[23] Filippov S, Jansson M, Stehr J E, Palisaitis J, Persson P O Å, Ishikawa F, Chen W M and Buyanova I A 2016 Strongly polarized quantum-dot-like light emitters embedded in GaAs/GaNAs core/shell nanowires *Nanoscale* **8** 15939–47

[24] Suzuki H, Sakai K, Haraguchi T, Yamauchi T, Hijii M, Maeda K and Ikari T 2014 Effects of nitrogen precursor on the Au-assisted vapor–liquid–solid growth of GaAs(N) nanostructures *J. Cryst. Growth* **386** 100–6

[25] Koppka C, Paszuk A, Steidl M, Supplie O, Kleinschmidt P and Hannappel T 2016 Suppression of Rotational Twin Formation in Virtual GaP/Si(111) Substrates for III–V Nanowire Growth *Cryst. Growth Des.* **16** 6208–13

[26] Steidl M, Koppka C, Winterfeld L, Peh K, Galiana B, Supplie O, Kleinschmidt P, Runge E and Hannappel T 2017 Impact of Rotational Twin Boundaries and Lattice Mismatch on III–V Nanowire Growth *ACS Nano* **11** 8679–89

[27] Kuang Y J, Sukrittanon S, Li H and Tu C W 2012 Growth and photoluminescence of self-catalyzed GaP/GaNP core/shell nanowires on Si(111) by gas source molecular beam epitaxy *Appl. Phys. Lett.* **100** 053108

[28] Sukrittanon S, Dobrovolsky A, Kang W-M, Jang J-S, Kim B-J, Chen W M, Buyanova I A, Tu C W and Kuang Y J 2014 Growth and characterization of dilute nitride GaNxP1−x nanowires and GaNxP1−x/GaNyP1−y core/shell nanowires on Si (111) by gas source molecular beam epitaxy *Appl. Phys.*

Lett. **105** 072107

[29] Sköld N, Wagner J B, Karlsson G, Hernán T, Seifert W, Pistol M-E and Samuelson L 2006 Phase segregation in AlInP shells on GaAs nanowires. *Nano Lett.* **6** 2743–7

[30] Jiang N, Wong-Leung J, Joyce H J, Gao Q, Tan H H and Jagadish C 2014 Understanding the true shape of Au-catalyzed GaAs nanowires *Nano Lett.* **14** 5865–72

[31] Sibirev N V, Timofeeva M A, Bol'shakov A D, Nazarenko M V and Dubrovskiĭ V G 2010 Surface energy and crystal structure of nanowhiskers of III–V semiconductor compounds *Phys. Solid State* **52** 1531–8

[32] Jiang N, Wong-Leung J, Joyce H J, Gao Q, Tan H H and Jagadish C 2014 Sup.Info: Understanding the True Shape of Au-Catalyzed GaAs Nanowires *Nano Lett.* **14** 5865–72

[33] Davidson F M, Lee D C, Fanfair D D and Korgel B a. 2007 Lamellar twinning in semiconductor nanowires *J. Phys. Chem. C* **111** 2929–35

[34] Algra R E, Verheijen M a, Borgström M T, Feiner L-F, Immink G, van Enckevort W J P, Vlieg E and Bakkers E P a M 2008 Twinning superlattices in indium phosphide nanowires. *Nature* **456** 369–72

[35] Glas F, Harmand J-C and Patriarche G 2007 Why Does Wurtzite Form in Nanowires of III-V Zinc Blende Semiconductors? *Phys. Rev. Lett.* **99** 146101

[36] Dubrovskii V G 2015 Theory of VLS Growth of Compound Semiconductors *Semiconductors and Semimetals* pp 1–78

[37] Shokhovets S, Supplie O, Koppka C, Krischok S and Hannappel T 2018 Optical constants and origin of the absorption edge of GaPN lattice-matched to Si *Phys. Rev. B - Condens. Matter Mater. Phys.*

[38] Dobrovolsky A, Sukrittanon S, Kuang Y J, Tu C W, Chen W M and Buyanova I A 2014 Raman spectroscopy of GaP/GaNP core/shell nanowires *Appl. Phys. Lett.* **105** 193102

[39] Vorlíček V, Gregora I, Riede V and Neumann H 1988 Raman scattering study of GaP:N epitaxial layers *J. Phys. Chem. Solids* **49** 797–805

[40] Buyanova I A, Chen W M, Goldys E M, Xin H P and Tu C W 2001 Structural properties of a GaNxP1-x alloy: Raman studies *Appl. Phys. Lett.* **78** 3959–61

[41] Loudon R 1964 Selection rules for defect-activated lattice bands and vibronic transitions in face-centred cubic, diamond and zinc blende lattices *Proc. Phys. Soc.* **84** 379–88

[42] Yoon S, Seong M J, Geisz J F, Duda A and Mascarenhas A 2003 Evolution of electronic states in GaPN studied by resonant Raman scattering spectroscopy *Phys. Rev. B* **67** 235209

[43] Christian T M, Fluegel B, Beaton D A, Alberi K and Mascarenhas A 2016 Bismuth-induced Raman modes in GaP 1− x Bi x *Jpn. J. Appl. Phys.* **55** 108002

[44] Prévot B and Wagner J 1991 Raman characterization of semiconducting materials and related structures *Prog. Cryst. Growth Charact. Mater.* **22** 245–319

[45] Jussila H, Yu K M, Kujala J, Tuomisto F, Nagarajan S, Lemettinen J, Huhtio T, Tuomi T O, Lipsanen H and Sopanen M 2014 Substitutionality of nitrogen atoms and formation of nitrogen complexes and point defects in GaPN alloys *J. Phys. D. Appl. Phys.* **47** 075106

[46] Dagnelund D, Buyanova I A, Wang X J, Chen W M, Utsumi A, Furukawa Y, Wakahara A and Yonezu H 2008 Formation of grown-in defects in molecular beam epitaxial Ga(In)NP: Effects of growth conditions and postgrowth treatments *J. Appl. Phys.* **103**

[47] Thinh N Q, Vorona I P, Buyanova I A, Chen W M, Limpijumnong S, Zhang S B, Hong Y G, Xin H P, Tu C W, Utsumi A, Furukawa Y, Moon S, Wakahara A and Yonezu H 2005 Properties of Ga-interstitial defects in Al xGa 1-xN yP 1-y *Phys. Rev. B - Condens. Matter Mater. Phys.* **71** 1–9

[48] Wang X J, Puttisong Y, Tu C W, Ptak A J, Kalevich V K, Egorov A Y, Geelhaar L, Riechert H, Chen W M and Buyanova I A 2009 Dominant recombination centers in Ga(In)NAs alloys: Ga interstitials *Appl. Phys. Lett.* **95** 95–8

[49] Xin H P, Tu C W, Zhang Y and Mascarenhas a. 2000 Effects of nitrogen on the band structure of GaN[sub x]P[sub 1−x] alloys *Appl. Phys. Lett.* **76** 1267

[50] Baillargeon J N, Cheng K Y, Hofler G E, Pearah P J and Hsieh K C 1992 Luminescence quenching and the formation of the GaP1-xN x alloy in GaP with increasing nitrogen content *Appl. Phys. Lett.* **60** 2540–2

[51] Zhang Y, Fluegel B, Mascarenhas a., Xin H and Tu C 2000 Optical transitions in the isoelectronically doped semiconductor GaP:N: An evolution from isolated centers, pairs, and clusters to an impurity band *Phys. Rev. B* **62** 4493–500

[52] Kent P R C and Zunger A 2001 Theory of electronic structure evolution in GaAsN and GaPN alloys *Phys. Rev. B* **64** 115208

[53] Buyanova I a, Chen W M and Tu C W 2003 Recombination processes in N-containing III – V ternary alloys *Solid. State. Electron.* **47** 467–75

[54] Buyanova I A, Rudko G Y, Chen W M, Xin H P and Tu C W 2002 Radiative recombination mechanism in GaN[sub x]P[sub 1−x] alloys *Appl. Phys. Lett.* **80** 1740

[55] Thomas D G and Hopfield J J 1966 Isoelectronic traps due to nitrogen in gallium phosphide *Phys. Rev.* **150** 680–9

[56] Wang R, Zhou G, Liu Y, Pan S, Zhang H, Yu D and Zhang Z 2000 Raman spectral study of silicon nanowires: High-order scattering and phonon confinement effects *Phys. Rev. B* **61** 16827–32

[57] Peternai L, Kovac J, Jakabovic J, Gottschalch V and Rheinlaender B 2006 Investigation of GaNxP1-x/GaP LED structure optical properties *J. Electron. Mater.* **35** 654–7